Astron. Astrophys. 360, 896–910 (2000)

ASTRONOMY AND ASTROPHYSICS

EISily looking for distant clusters of galaxies – a new algorithm and its application to the EIS-wide data

C. Lobo[1,2], **A. Iovino**[1], **D. Lazzati**[1], **and G. Chincarini**[1]

[1] Osservatorio Astronomico di Brera, Via Brera 28, 20121 Milano, Italy
[2] Observatório Astronómico de Lisboa, Tapada da Ajuda, 1349-018 Lisboa, Portugal

Received 27 April 2000 / Accepted 16 June 2000

Abstract. We present a new algorithm to search for distant clusters of galaxies on catalogues deriving from imaging data, as those of the ESO Imaging Survey.

Our algorithm is a matched filter one, similar to that adopted by Postman et al. (1996), aiming at identifying cluster candidates by using positional and photometric data simultaneously. The main novelty of our approach is that spatial and luminosity filter are run separately on the catalogue and no assumption is made on the typical size nor on the typical M^* for clusters, as these parameters intervene in our algorithm as typical angular scale σ and typical apparent magnitude m^*. Moreover we estimate the background locally for each candidate, allowing us to overcome the hazards of inhomogeneous datasets. As a consequence our algorithm has a lower contamination rate - without loss of completeness - in comparison to other techniques, as tested through extensive simulations. We provide catalogues of galaxy cluster candidates as the result of applying our algorithm to the I–band data of the EIS-wide patches A and B.

Key words: methods: numerical – galaxies: clusters: general – cosmology: large-scale structure of Universe

1. Introduction

The quest for high–redshift ($z \gtrsim 0.5$) clusters of galaxies has recently received a lot of attention, and several search methods have been put forward. The mere existence of rich clusters of galaxies at very high redshifts is cosmologically relevant and their importance as a discriminant among different theoretical cosmological models is widely acknowledged (see e.g. Viana & Liddle 1996; Carlberg et al. 1997; Bahcall et al. 1997; Bartelmann et al. 1998). On the other hand, a detailed study of the properties of clusters, as well as of their member galaxies, at high redshifts and the confrontation of these with local well-known systems gives precious insight on their formation and on the evolution of their properties with redshift and environment (Dressler et al. 1997; van Dokkum et al. 1998a, 1998b; Smail et al. 1998; Morris et al. 1998; Stanford et al. 1998 and references therein). The now well-established evolution of galaxies with redshift still lacks a clear understanding of the physical processes that guide it: clusters are privileged observational targets to distinguish between intrinsic and environmental effects.

To perform the search for distant clusters of galaxies, various authors have been taking advantage of several windows in the spectral emission of the different cluster components, namely galaxies and gas, and applying the best suited method in each case. Thus, optical, near IR, X–ray and even variations in the cosmic microwave background emission have been used to detect cluster candidates at distant redshifts. All different methods have advantages and drawbacks and the key is to view them as complementary. Describing each one of them and presenting their respective pros and cons is beyond the scope of this paper. Nevertheless, it is useful to recall what has been done up to now, in order to place our work in the actual scenario of these researches.

Among the different techniques that basically search for surface density enhancements on the galaxy 2D spatial distribution - adding or not magnitude information as well -, some of the most popular ones are the application of adapted filters (e.g. kernel, wavelets, matched filters), counts-in-cells techniques, percolation algorithms or even, lately, Voronoi tessellation, on optical photometric data (e.g. Schectman 1985; Lumsden et al. 1992; Dalton et al. 1994; Escalera & MacGillivray 1995, 1996; Pisani 1996; Lidman & Peterson 1996; Fadda et al. 1998; Postman et al. 1996; Gal et al. 2000; Ostrander et al. 1998), and on NIR data (Stanford et al. 1997; Mendes de Oliveira et al. 1998, Ramella et al. 1998). Apart from these more or less elaborate techniques, simpler high-contrast methods still prove to be successful (Couch et al. 1991), but they probably don't sample adequately the full distant cluster population and their selection criteria are not well defined. Some of these algorithms benefit also from - or are mainly based upon - multiband colour information that helps isolating red galaxies at higher redshifts (Gladders & Yee 2000).

Very significant results have been achieved *via* the search for sources of extended emission in X–ray surveys with detection algorithms which are designed to probe a broad range of cluster parameters such as X–ray flux, surface brightness and morphology (e.g. Henry et al. 1992 with EMSS; RIXOS by Castander et al. 1995; the RDCS by Rosati et al. 1995, 1998; NEP by Henry et al. 1997; Gioia 1997; WARPS by Scharf et al. 1997;

Send offprint requests to: C. Lobo (lobo@oal.ul.pt)

Jones et al. 1997b; SHARC by Collins et al. 1997; the BCS by Ebeling et al. 1998; the CfA large area survey by Vikhlinin et al. 1998a, 1998b; REFLEX by Böhringer et al. 1998).

Other emerging strategies for cluster search include: the detection of extragalactic background light fluctuations in shallow optical images (Dalcanton 1996; Zaritsky et al. 1997); deep imaging around privileged sites of density enhancements such as distant powerful radio-galaxies or radio-loud quasars (e.g. Le Fèvre et al. 1996; Deltorn et al. 1997); narrow–band imaging to search for concentrations of Ly–α emitters around previously known weak radio QSO's at high redshift (e.g. Pascarelle et al. 1996; Campos et al. 1999). Recently, the detection of decrements in the cosmic microwave background radio emission were also attributed to the presence of distant gaseous systems, possibly clusters (Jones et al. 1997a; Richards et al. 1997), that scatter the microwave background radiation *via* the Sunyaev–Zel'dovich effect (Sunyaev & Zel'dovich 1980). One should mention, though, that these strategies for cluster search refer to $z > 2$ systems and we ignore *"whether these are massive, collapsed systems, groupings within unvirialized "sheets" of galaxies, or collections of "protogalactic" fragments destined to merge into single, more massive galaxies"* (Dickinson 1996).

If one aims at producing statistically significant results, a good catalogue of clusters, preferably spanning a large interval of redshift, obtained using well defined selection criteria, over a reasonable sky area, is needed. Our algorithm, by uniformly detecting clusters over a wide range of redshifts and cluster sizes, is well suited to provide such a catalogue. We stress that it does not aim, however, at performing accurate estimates of neither the redshift nor the richness of the cluster candidates.

The ESO Imaging Survey (EIS, Renzini & da Costa 1997), covering a final area of 17 square degrees of the southern sky in the I-band, up to limiting magnitude $I \sim 23$, provided us with a good opportunity to produce such a catalogue. We have developed an automated cluster search algorithm and applied it to the catalogues derived from the EIS imaging data to obtain a reliable set of cluster candidates up to estimated $z \sim 1.1$. Having a list of robust candidates is highly desirable, before proceeding to the spectroscopic observations with very large telescopes, and our algorithm has a high success rate - that is, a high completeness level - without being overwhelmed by contamination in the form of spurious detections. We have already selected three of the highest redshift candidates ($z \geq 0.5$) and performed the spectroscopic follow-up with VLT, confirming their real existence as physically bound systems (discarding the possibility of false chance alignments) and determined their distance/redshift with accuracy.

In this paper we describe our algorithm in Sect. 2, stressing its strong points and advantages relatively to others present in the literature. Applying it to the EIS-wide data of patches A and B produced a catalogue of candidate clusters of galaxies that we present in Sect. 3. This set is quite different from the one produced by the EIS–team of ESO for the same original data set but using a different approach and in Sect. 4 we fully investigate all possibilities that may account for such a discrepancy. Final remarks are given in Sect. 5.

We shall use $H_0 = 50\,\mathrm{km\,s^{-1}Mpc^{-1}}$ and $q_0 = 0.5$ throughout this paper, unless explicitly stated otherwise.

2. Our new algorithm

In their pioneering work on the Palomar Distant Cluster Survey, Postman and collaborators (Postman et al. 1996, P96 hereafter) wrote a matched filter algorithm to identify cluster candidates by using positional and photometric data simultaneously. Slight variants have been proposed hence, with differences lying in some details of the detection processes (Kawasaki et al. 1998) or in the generalization of the algorithm so as to render it applicable to any type of survey data (Kepner et al. 1999). Our work, instead, tries to improve on the P96 algorithm in the sense of removing the *a priori* assumptions that are implicit in the Postman et al. technique.

The P96 algorithm relies on the choice of both a given cluster profile - modified–Hubble or King–like (hereafter often referred to as King filter for simplicity) - with a typical cluster scale - the core radius r_c - and a cut–off radius, and of a typical M^* - the chosen parameterization of the Schechter function. Both quantities, r_c and M^*, are rigidly coupled to detect cluster candidates and assign them a tentative redshift. Each one of these quantities being a function of distance (and thus cosmology), their implementation on any algorithm implies a dependence on the adopted cosmology and on the chosen amount of evolution, not to mention the dependence on the particular values actually chosen for r_c and M^*.

In our new algorithm the spatial and luminosity part of the filter are run separately and successively on the catalogue, with no assumption on the typical size or typical M^* for clusters. In fact, these parameters intervene in our algorithm only as a typical angular scale and typical apparent magnitude m^*, bearing no ties to fixed physical scales nor to absolute magnitudes through redshift dependence. This has the consequence of removing the need for a choice of fixed physical values for these two quantities, and for a choice of evolutionary models. Moreover, the fact of not coupling the space and the luminosity parameters also enables us to reach higher values of completeness: a candidate can be retrieved even if it does not flag a maximum likelihood at the very same redshift value simultaneously for both the space and the luminosity distributions (a situation that would lower its global likelihood when using the P96 algorithm).

One further advantage consists in the local estimate of the background for each cluster candidate. In the approach of P96, the magnitude distribution is assumed constant all over the catalogue and so is the background spatial density. This may be hazardous especially in what concerns the spatial part, where local inhomogeneities may hamper the detection in shallower regions of the catalogue. Due to varying observing conditions, a part of the EIS data, at least, is reported to be non uniform (Olsen et al. 1999b), so this feature of our algorithm is of great help, as it allows us to tackle the problems of inhomogeneous data sets and to achieve higher levels of completeness.

In our algorithm local enhancements in the projected galaxy density are first selected through the Gaussian filtering, and a

"spatial probability" of them being spurious is computed. Subsequently, the maximum-likelihood "filtering" on the apparent magnitudes searches for the presence of a Schechter distribution superimposed on the local background (which follows a power–law instead). This second step leads to the assessment of a corresponding "luminosity probability" that, multiplied by the spatial one, produces the final probability of each candidate being a spurious one. This means that the lower this value, the more confident the candidate. Notice also that this final quantity is always lower than either one of the partial spatial or luminosity probabilities as it is their product.

We will now discuss in detail the components of the algorithm.

2.1. The spatial filter

In the spatial part we have chosen to work with a Gaussian filter. This choice, while avoiding to specify too particular a shape for the profile of the cluster candidates, brings along all the advantages and favorable mathematical properties of the Gauss function. It is worth remembering that the gaussian function in Fourier space is more compact than the King function. As a consequence the convolution with a random distribution of galaxies (a white noise in fourier space) will produce less spurious detections for the Gauss filter than for the King filter.

Regarding completeness, it can be interesting to show, using simulations, the relative advantages of the Gaussian filter with respect to the King filter. A simple way of doing it is to simulate an area with randomly distributed field galaxies where to embed clusters, and apply to this area the two spatial filters in question to perform cluster detection and to compare directly completeness for both of them.

Comparing the two filters is not straightforward, though: their shapes are intrinsically different so that there is no direct correspondence between the respective typical scales (r_c and σ_{ang}). The King–like profile has a slimmer central peak with broad wings while the Gaussian shows the well known bell–shaped form. However, when cross-correlating the two filters, the highest signal is achieved if we consider $\sigma_{ang} \sim 2.52 \times r_c$, suggesting that a factor of 2.52 should be used in the simulations when comparing the relative efficiency of the Gauss *versus* King filters. Besides, since when searching for a spatial density enhancement one has to move in steps of dimension comparable to the typical scale of the filter, this also implies that the Gaussian filtering requires a factor of $(2.52)^2 \simeq 6$ less search points with respect to the King filtering.

As we have already mentioned, in our search we will not fix any typical physical size for our filter, but we will use, instead, a range of angular sizes σ_{ang}, namely from ~ 0.35 up to ~ 1.42 arcmin in five steps of ratio $\sqrt{2}$. These values were chosen bearing in mind the range of reasonable dimensions of the cluster candidates spanning the redshift interval that we expect to probe with the EIS data ($z \lesssim 1.2$). The corresponding five r_c values to be used in the spatial search with the King–like filter are those obtained using the relationship $\sigma_{ang} \sim 2.52 r_c$.

2.1.1. Simulations

The simulations performed for this comparison were done as a function of the signal-to-noise threshold chosen, of the cluster profile, richness and redshift.

As the final goal was to apply our algorithm to the EIS data, to simulate the galaxy background distribution we used the data from the EIS itself (see Sect. 3), by random shuffling galaxy positions and magnitudes within the limits of the survey.

The contamination rates were assessed by running the Gaussian filter and the King filter on these pure background fields.

In what regards completeness, this rate was assessed by running the two filters on the background fields plus cluster galaxies. This means that, for each simulation, a cluster of galaxies with different characteristics was placed randomly within each background frame, with the only constraint of being at adequate distance from the frame borders (i.e. a distance larger than both 10 times the σ_{ang} used for the search as well as 5 times the angular size of the embedded cluster), in order to avoid border effects. The characteristics of the clusters were defined according to the following prescription:

1. The cluster mean redshift: ranging from $z = 0.2$ till $z = 1.2$ at intervals of $\Delta z = 0.2$.
2. The surface density profile: a power law in radius of the form r^β. The index β was set to three different values (0, -1 and -2) when testing the spatial filter only (as is the case of this section). But it was fixed to the typical in–between case $\beta = -1.4$ for the overall simulations (further ahead, in Sect. 2.5, when we will apply the complete algorithm - that is, both spatial and luminosity filters - to the mock catalogues); this provided a compromise that also allowed a direct comparison with the P96 results. Furthermore, we introduced a small central smoothing region in the profile, with the typical size of a cluster cD galaxy ($r_{smooth} \sim 35$ kpc, the average diameter of the two central giant galaxies in Coma, as provided by the NED-database), to avoid a cusp. Both r_{smooth} and the total radial size of the cluster, 1 Mpc, were translated into the corresponding angular sizes according to the redshift chosen in item 1. Doubling the cluster size to 2 Mpc did not change the results of our simulations in terms of completeness.
3. The luminosity function - a Schechter, which is generally adopted to describe the luminosity distribution of cluster galaxies (Schechter 1976), but with parameters determined by Colless (1989) for a set of 14 clusters of mean redshift $\langle z \rangle \simeq 0.0851$ observed in the B_J band. Thus, the faint end slope is $\alpha = -1.25$ and the characteristic apparent magnitude, at that mean redshift, is $m_I^* = 14.8$ when converted to the I-band (Fukugita et al. 1995). The m_I^* used in each simulation was changed according to the redshift (item 1) and to the k-correction applied (see item 5 below).
4. The richness, as given by n^*, the number of galaxies brighter than the characteristic magnitude m^*. Three cases were considered: $n^* = 30, 50$ and 80 (following Schechter 1976). These can be roughly identified with Abell richness classes $R = 1$, 2 and 3 (Abell 1958; see also Bahcall 1988).

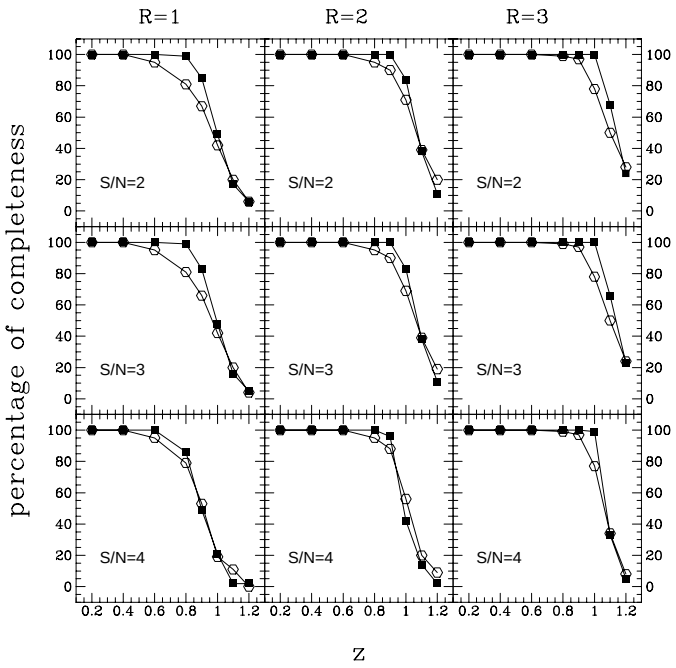

Fig. 1. Comparative performance, in completeness rate, between the spatial filter used in our new algorithm with the five adopted angular widths (σ_{ang}) - filled squares - and the P96 King–like spatial filter with the corresponding five core radii - empty circles - such that $r_c = 1/2.5\sigma_{ang}$. Each point represents the mean value of a set of 100 bootstrap simulations. Clusters are elliptical dominated, have radial profile r^{-1} and richness class $R \sim 1$ (left), $R \sim 2$ (center), and $R \sim 3$ (right). See text for further details.

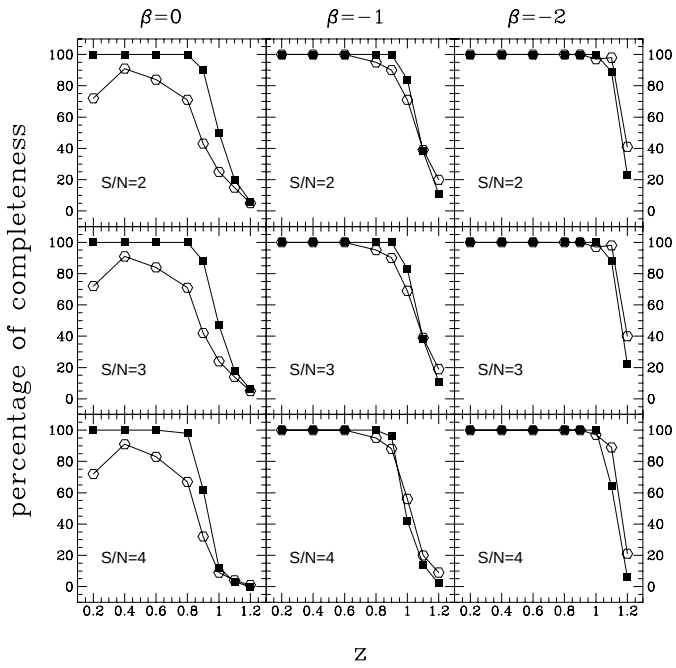

Fig. 2. Same as Fig. 1 but now the richness class has been fixed to $R = 2$ and different r^{β} radial profiles are compared in terms of filter completeness performance. Left panels represent $\beta = 0$ clusters, in the middle stand $\beta = -1$ clusters and the right panels show results for $\beta = -2$, steeper profile, clusters.

5. The dominant morphological type, as implied by the k-correction that is used. Actually only one extreme case was tested: clusters entirely composed of elliptical galaxies. We deliberately chose to ignore both the evolutionary corrections and the possibility of having later morphological types as the cluster dominant population, since this would correspond to a more favorable scenario of rendering cluster members brighter, which would only facilitate their detection. k-corrections have been provided by the spectro-photometric evolutionary model *PEGASE* of Fioc & Rocca-Volmerange (1997) tuned to the cosmology parameters adopted.

Once these characteristics are fixed, we can compute, for each cluster, the number of member galaxies that are observable within the apparent magnitude limit. Positions and magnitudes are next assigned to these cluster galaxies by random shots drawn from items 2 and 3, respectively.

This was done in sets of 100 simulations and the two spatial filters were applied to these mock catalogues. Both field and cluster galaxies were limited to a magnitude cut–off of I=22.0, the one we adopted also for the EIS data.

In terms of completeness, the results are summarized in Figs. 1 and 2.

According to the plots in Figs. 1 and 2, the comparative performance in completeness rate shows that the Gaussian filter is more efficient in most of the cases than the King filter, and this is especially true in particular in the difficult case when the cluster profile is less peaked.

2.2. The luminosity filter

To assess the signal given by the luminosity information we apply a maximum-likelihood technique on the apparent magnitude distribution of the candidates previously found with the spatial filter. We use as functional form for the luminosity function a Schechter (1976) function expressed in apparent magnitudes, thus avoiding the P96 choice of an intrinsic M^* and the choice of a given cosmology (H_0 and q_0) and morphological content (translated in the assumption of a given k-correction and, eventually, of an e-correction as well). Also, unlike P96, we have decided to implement the generalized treatment for this likelihood filter, following Schuecker & Böhringer (1998). This complete treatment uses the exact mathematical equations, allowing to keep track of all possible errors that would affect any eventual direct redshift estimate (like the one performed by P96). It does not add major computational effort nor time. Besides, it also renders unnecessary the final *"cluster signal correction"* demanded by the complex approximations of the P96 procedure.

We thus took Eq. (8) of Schuecker & Böhringer (1998) and adapted it to compute the likelihood for this luminosity part of our algorithm. Notice that, as we decouple it from the spatial part, the galaxy distribution profile is suppressed from the original formula so that the final log-likelihood ratio, for a given m^*, is:

$$\ln\left(\frac{L_{S+bkg}}{L_{bkg}}\right) = \sum_{i=1}^{N} \ln\left[\frac{N\,-\,\Lambda}{N}\left(1+\frac{\Lambda\,\phi(m_i-m^*)}{(\,N\,-\,\Lambda)\;b(m_i)}\right)\right] \quad (1)$$

where L stands for the likelihood function, S and $\phi(m_i - m^*)$ refer to the Schechter function parameterized by a given m^*, bkg stands for the background galaxies and $b(m)$ for the differential magnitude number counts of the background galaxies; $b(m)$ is mathematically described by the fit to the magnitude distribution of all galaxies in the catalogue. N is the total number of cluster and field galaxies present inside a $2.5\sigma_{ang}$ radius circle, where we also estimate a coarse richness parameter Λ (as will be detailed in Sect. 2.3).

Note that ϕ has been normalized, i.e.:

$$\int_0^{m_{lim}} \phi(m-m^*)\,dm \;=\; 1 \quad (2)$$

m_{lim} being the limiting magnitude of the catalogue.

For each candidate we compute the log-likelihood ratio (Eq. 1) for different m^* values, set within the limits of magnitude of the galaxy catalogue by steps of 0.1 magnitude. The slope of the Schechter function is fixed to $\alpha = -1.25$, according to the mean value derived by Colless (1989) and in agreement with typical cluster luminosity function parameters found in the literature since the work of Schechter (1976). By identifying the absolute maximum in the distribution of the log-likelihood ratios relative to all m^*, we automatically select the output m^* for that candidate.

2.3. Detailed description of the algorithm steps

In this section we present a detailed description of the way the algorithm works when applied to the data.

We note that we shall often interchange probability with the complementary Gaussian percentile and the associated level of standard deviations, referred to as S/N throughout this paper. This approximation was used also in P96 so, by adopting it as well, we render comparisons among our results easier.

The algorithm starts off by reading the coordinates and magnitudes of the galaxies present in a magnitude limited catalogue. Then, for each one of the five selected angular apertures σ_{ang} of the Gaussian, the code:

1. Builds the search grid for the spatial filter analysis. The spacing between adjacent grid points is σ_{ang} but no grid point is allowed within $3\sigma_{ang}$ of the catalogue's borders in right ascension nor in declination.
2. Computes a first hand estimate of the local background density associated to each grid point by counting the number of galaxies in a circle with a $6\sigma_{ang}$ radius centered at the grid point in question. (All cases of grid points distant less than $6\sigma_{ang}$ from the catalogue's borders are obviously corrected by shifting the circle.) Notice that, in this way, the background spatial density is not assumed constant all over the catalogue, but is estimated around each point. This characteristic proves to be particularly efficient in dealing with data - like those of EIS in at least some of the patches - where varying observing conditions result in non homogeneity of the galaxy catalogue (Olsen et al. 1999b).
3. Performs the Gaussian filtering at each grid point considering all galaxies within $3\sigma_{ang}$ from it and weighing their relative position through the Gauss function. The resulting output signal is normalized (respective mean subtracted and division by the corresponding standard deviation), obtaining the S/N appropriate for each grid point.
4. Selects all grid points which flag a local maximum, i.e., for which the spatial signal is greater than that of all their immediate grid neighbours. No points at the extremes of the grid are allowed in this choice, thus avoiding "border effects". The signal must also be above a given threshold, imposed as an input in the programme. We set this spatial detection threshold to 2.5 (the equivalent to the 98th percentile).
5. For these maxima, our algorithm proceeds to the fine centrage: the Gaussian filtering is redone, maintaining the filter angular size, but building a finer grid in an iterative procedure (down till an eighth of σ_{ang}) around the tentative candidate. The fine tuned center is finally chosen as the position where the spatial signal is maximized in the ensemble of the points of this denser grid.
6. The five different scale catalogues are cross-correlated in order to remove double detections. Detections are considered double if the distance between their centers is lower than or equal to the mean of their scales. In this case, only the highest signal detection is kept.
7. For each selected candidate, the next step is to obtain a preliminary estimate of its richness, Λ, to be used in the computations of the likelihood of the luminosity part (see Eq. 1). Λ is the approximate number of galaxies statistically belonging to the cluster candidate. We obtain it by subtracting to the N galaxies inside a $2.5\sigma_{ang}$ radius the local background, estimated in a annulus around each candidate. This ring has an inner radius of $5\sigma_{ang}$ and its area totals 0.06 deg^2. These values were chosen after evaluating the galaxy density distribution around several candidates in the final EIS catalogue.
8. For each candidate we compute the log-likelihood ratio (Eq. 1) for the set of m^* values and determine the one that maximizes it. The probability associated to this value is obtained by bootstrap: the catalogue is randomized, the spatial filter is run on it and the distribution of the log-likelihood for the flagged spatial detections is computed thus allowing an estimate of the probability of having an L_{max} greater or equal than that measured for our candidate.
9. At this point we possess the σ_{ang} and m^* that independently maximize both the spatial and the luminosity signals and their respective significance, P_{space} and P_{lum}. We can combine these probabilities to obtain a final global probability, P_{tot}, for the detection of each cluster candidate. This is simply done by multiplying P_{space} by P_{lum}.

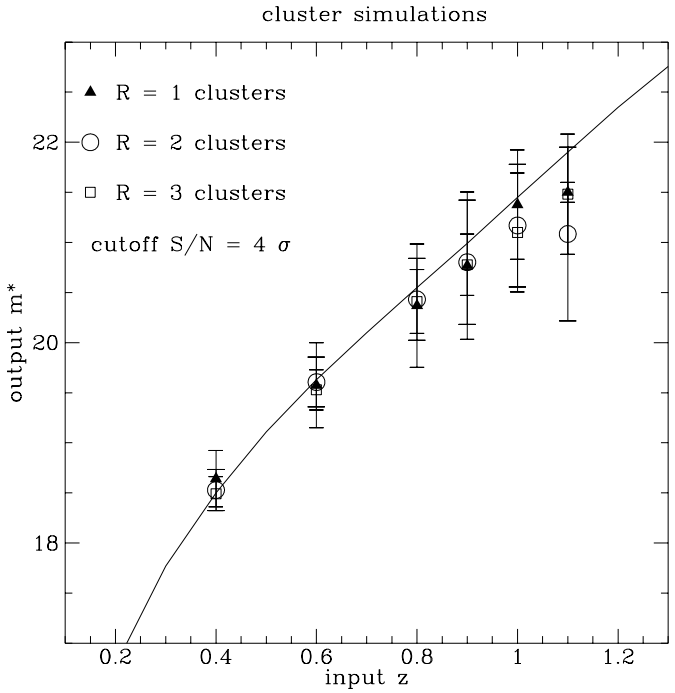

Fig. 3. Results from the simulations (that allowed us to assess the overall completeness rate - see Sect. 2.5) showing the comparison between the redshift value of the simulated clusters and the output m^* obtained from our algorithm. The curve shows the relationship between z and m^* used to define the input m^* in our simulations (see text for further explanations). Each point is the mean of 100 simulations. 1σ error bars are drawn.

2.4. Richness estimate

The estimate of the richness of our cluster candidates is an important step, as we would like to quantify the percentage of groups *versus* rich clusters that we will be detecting.

Whichever richness estimate one decides to adopt, a necessary step is the determination of a physical radius for each cluster candidate which, in turn, requires the estimate of its redshift. Unlike P96, our method does not provide a direct estimate of the redshift for our candidates. We obtained such estimate using m^* and its relationship to M^*, whose adopted value is that reported by Colless (1989), to be redshifted and corrected using the k-corrections typical of ellipticals, as determined by Fioc & Rocca-Volmerange (1997). Simulations show that the value of m^* obtained through our algorithm retrieves well the M^* introduced in the simulations - see Fig. 3. On the contrary, the value of σ_{ang} retrieved by our algorithm does not correlate well with redshift: the angular size chosen by the algorithm has a large scatter with respect to the physical size of the clusters entered in the simulations.

Having thus obtained a rough estimate of the candidate's redshift, we can also estimate its richness, adopting the $N_{0.5}$ parameter proposed by Bahcall (1981). It consists in counting the number of cluster member galaxies brighter than $m_3 + 2$ (where m_3 is the magnitude of the third brightest cluster galaxy), located within a projected radius of 0.5 Mpc from the cluster center, the typical size of a cluster X–ray emitting region. Background correction is estimated from similar counts performed in the entire catalogue region, using 0.2 magnitude bins. $N_{0.5}$ was found to be well correlated with the system's velocity dispersion v_r by Bahcall (1981, see also e.g. Alonso et al. 1999 for further studies on this type of correlation) for a sample of 26 nearby clusters ranging from rich systems ($v_r \sim 1500 \mathrm{km\,s^{-1}}$) to small groups of galaxies ($v_r \sim 100 \mathrm{km\,s^{-1}}$) and has already been used in the literature for richness estimates of distant clusters (Deltorn et al. 1997). It has the advantage of avoiding the higher uncertainties in background subtraction present when adopting the standard Abell (1958) estimate, which is performed within a radius of 3 Mpc (see e.g. P96 for comments on this). In fact, $N_{0.5}$ is relatively insensitive to uncertainties in either the background correction or in the exact position of the cluster center (Bahcall 1981). $N_{0.5}$ can be translated into the typical Abell richness classes using the indicative relation given by Bahcall (1981), $N_{Abell} \simeq 3.3 \times N_{0.5}$, and then checking Table 1 of Bahcall (1988). This means that e.g. $N_{0.5} < 15$ corresponds to Abell richness class $R \sim 0$, while $N_{0.5} > 24$ is equivalent to $R \gtrsim 2$.

2.5. Expected final overall rates of completeness and contamination – simulations

We ran a new set of extensive simulations in order to assess the overall efficiency of the algorithm. The layout of these simulations being the same as the ones that were used for estimating the completeness and contamination rates of the spatial filter alone (see Sect. 2.1.1), we shall not repeat their details. Here, it will be enough to mention that the mock catalogues (pure field for contamination rates or field plus cluster galaxies for completeness purposes) were now submitted to the algorithm, and not only to its spatial filter as had been done in Sect. 2.1.1.

The results regarding the overall completeness rates are shown in Fig. 4. Even setting the detection threshold at $S/N \sim 4.0$ - which renders contamination rates negligible (see below for the final overall rate of contamination directly assessed on the EIS data) - we are able to achieve a completeness of $\sim 95\%$ until $z \sim 0.9$ for richness 2 Coma-like clusters, and of $\sim 97\%$ up to $z \sim 0.8$ for poorer richness class 1 systems. For $R = 3$ clusters such high values of completeness hold even in the redshift bin $z \sim 1.0$, always for the no-evolution case. These results improve on the values obtained using the P96 algorithm (see their Fig. 20). In fact, while we set the Schechter slope of the simulated clusters to a steeper value (-1.25 instead of -1.1), the fact of having adopted a brighter magnitude limit (22.0 *versus* P96's 22.5) renders a direct comparison of both works plausible. We checked this by integrating both Schechters for the two magnitude limits, thus getting 38(us) *versus* 50(P96) galaxies for R=1 clusters, 63 *versus* 82 galaxies for R=2 clusters, and 100 *versus* 131 galaxies for R=3 clusters. Moreover, do notice that the cut–off S/N is actually very different: while we set this threshold to 4σ, P96 report as detection limit the 95th percentile (i.e. approximately the 2σ level) in their simulations.

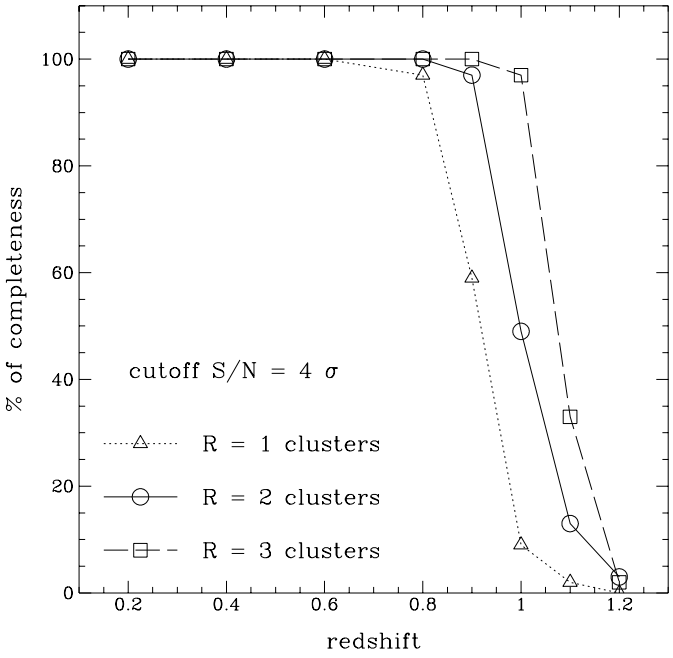

Fig. 4. Percentage of completeness for Abell richness classes $R = 1$ (poor), $R = 2$ (intermediate) and $R = 3$ (rich) clusters as established through simulations. Clusters have a power law radial profile of type $r^{-1.4}$, are dominated by ellipticals, and have a typical luminosity function as determined by Colless (1989). We applied elliptical k-corrections (Fioc & Rocca-Volmerange 1997) to cluster galaxies.

As for the expected contamination rate, we ran our algorithm on the EIS catalogue after having randomized galaxy positions and magnitudes. This time, no clusters were added to the galaxy background distribution, as we were interested in the false detection rate associated to a given threshold S/N. These simulations supply ~ 14 spurious candidates per square degree if the threshold is set at $S/N = 3$, and ~ 1.3 per square degree if it is set at $S/N = 4$. P96 report an estimated contamination rate for their final catalogue (of 79 candidates) of at most 30% in their 5.1 square degree area, corresponding to a surface density of contaminants of ~ 5 per square degree for PDCS. However, a direct comparison between the two results is very difficult since the data are different and the algorithms have very different selection methods.

3. The catalogues

Our final catalogues contain the following entries for each one of the candidate clusters found in EIS-wide patches A and B: right ascension and declination (equinox 2000), indicative angular size $2.5\sigma_{ang}$ (in arcmin), combined total probability expressed as a S/N, m^*, redshift and richness ($N_{0.5}$) estimates.

3.1. Defining our data set

ESO provides on the web the single frame catalogues for the even and the odd coverage of the EIS patches (http://www.eso.org/science/eis/). We thus had to assemble these data and build two galaxy catalogues (henceforth the even and the odd) for each entire patch, that were the basis for the cluster searches.

Table 1. Limits of the regions to be analyzed by our algorithm (coordinates are expressed in equinox J2000).

patch	α_{min} $(h\ m\ s)$	α_{max} $(h\ m\ s)$	δ_{min} $(o\ ,\ ,,)$	δ_{max} $(o\ ,\ ,,)$
A	22 35 31	22 49 41	-40 28 37	-39 27 36
B	00 44 30	00 54 01	-29 53 24	-29 17 24

After careful inspection of the EIS data characteristics, we decided to adopt the following parameters to define the galaxy catalogue on which to perform our automated search. The star/galaxy separation line was drawn at 0.9: only the objects with stellarity index lower than this value were kept, irrespective of their magnitude. Let us notice that this criterion slightly differs from that adopted by Olsen et al. (1999a, 1999b), where all the objects at magnitude fainter than 21 were kept, irrespective of their stellar index, introducing a sharp step at I=21 in the galaxy number counts.

We excluded objects with $f > 4$ and nflag/npix > 0.01 (where f are the SExtractor flags, npix the number of pixels above the analysis threshold and nflag the number of pixels flagged by WeightWatcher - see Nonino et al. 1999 for details). The layout of the EIS mosaic is such that adjacent odd/even frames have a small overlap at the edges, especially in declination and we further did cure double detections in frame borders (i.e. for pixel values $X \leq 100$, $X \geq 1950$, $Y \leq 300$ or $Y \geq 1600$) using a 2 arcsec separation cut–off.

We limited the data set to $18 \leq I \leq 22.0$, aiming at guaranteeing a high level of completeness of the data. We note that Nonino et al. (1999) estimate that the single-frame odd and even catalogues are 80% complete to $I = 23$ for a typical EIS frame.

Finally, and for technical reasons, we trimmed each patch so as to have clear-cut rectangular edges. This translates into the limits given in Table 1, and in the following number of galaxies: 57366 for patch A–even, 57553 for patch A–odd, 25456 for patch B–even and 25445 for patch B–odd. In summary, we have four catalogues, two (the even and the odd) for each patch, where we shall independently run our algorithm.

3.2. Defining our S/N thresholds

The choice of a threshold value in S/N for cluster detection has to be a compromise between the will to achieve a high level of completeness and the need to avoid unacceptable high values of contamination.

In Sect. 2.5 we have shown that a cut–off value of $S/N = 4\sigma$ gives a number of contaminants of ~ 1.3 per square degree, while guaranteeing a high level of completeness ($\geq 97\%$ for all three richness classes $R = 1 - 3$ up to a redshift of 0.8 - see Fig. 4).

If we had in our hands two good quality even and odd catalogues for each patch, we could just apply such cut–off on

both catalogues and get two final lists of cluster candidates that should differ by a small number, caused by false detections in regions where e.g. SExtractor detected spurious objects in the spikes of bright saturated stars or satellite tracks.

Unluckily, this does not appear to be the case for the data, especially in what concerns patch A, whose CCD frame quality is quite variable (Olsen et al. 1999b). As a result, applying a blind cut–off of 4σ to both catalogues would be too restrictive a choice, and therefore we decided to follow a more flexible approach.

For each patch we first built, for the corresponding even and odd galaxy catalogue, a catalogue of cluster candidates with a S/N cut–off of 3. Then, from these catalogues we selected:

Class 1 candidates: present in both even and odd catalogues (which implicitly means that they have $S/N \geq 3.0\sigma$ in both catalogues) with $S/N \geq 4.0\sigma$ in at least one of them;

Class 2 candidates: present in one catalogue only but having $S/N \geq 4.0\sigma$.

In this way, and for each patch, we do not reject those candidates that are present only in one catalogue; in fact, very often, these single detections include, other than flagrant false candidates, systems non detected in one of the catalogues due to shallower images, worse seeing conditions or general lower photometric quality.

In terms of contamination, our choice is equivalent to applying a $S/N \geq 4.0$ cut–off to the even/odd catalogues separately and the same holds for completeness, but with the further constraint for *class 1* candidates of being present also in the odd/even catalogue with $S/N \geq 3.0$ (no further constraint for *class 2* candidates).

3.3. Cluster candidates

3.3.1. Patch A

Class 1 candidates in patch A total 41 (see Table 2), which translates into a projected number density $\Sigma \sim 13$ clusters per square degree (this patch covers ~ 3 square degrees). Three further *class 1* candidates were detected in patch A but are not listed in Table 2. Two were cases of a bright star split into many objects and causing false detections, and a third one was a nearby low surface brightness galaxy again split into many components. The total expected number of spurious detections in this area (see Sect. 2.5), is < 4.

Table 2 lists, for each candidate, its right ascension, declination (both at the year 2000), a typical size ($2.5\sigma_{ang}$, where σ_{ang} is the size of the spatial detection filter in arcmin), the S/N in the even and odd galaxy catalogues, the output m^*, the estimated cluster redshift and the richness indicator $N_{0.5}$ (Bahcall 1981). The last column reports identifications with other catalogues, whenever is the case.

The indicated size is the mean value of what was measured from the even and odd catalogues respectively. The same was computed for all the other quantities in the Table (S/N excluded, obviously), except whenever at least one of the two next cases occurred: (1) The redshift estimates from the even and odd catalogues differed in absolute value by more than 0.1. This happened for a small percentage of the entries (8 over 41 i.e. 20%), suggesting that our *'a posteriori'* redshift estimate is quite robust "internally" (between even and odd catalogues). (2) The richness estimate was hampered because the candidate was attributed $m_3 + 2 > 22$ (the adopted magnitude limit) in the even catalogue (noted (e)) or in the odd (marked (o)) or in both ((eo)). In these cases, results issued from both even and odd catalogues were listed.

Furthermore, candidates marked with an asterisk have only a lower limit for the S/N, obtained using the spatial information alone. For these candidates we preferred to avoid quoting the total S/N as their P_{lum} was extremely low, possibly an artifact due to bad data quality: a careful inspection revealed that local faint galaxy counts were significantly below those of patch A as a whole thus causing, as a consequence, an overestimate of the significance of the bright galaxy excess.

As for *class 2* candidates in this patch, Table 3 lists 29 detections: those that survived a visual scrutiny aimed at rejecting obvious cases of false signals (satellite trails, bright star refraction spikes and other artifacts). For each cluster candidate the same quantities as in Table 2 are listed.

The reason for a candidate - not being an obvious artifact of the data - to be present only in one of the two catalogues of patch A has to be related to the worse quality of the corresponding CCD frames in the catalogue where it is missing. The variables at work are numerous (such as seeing conditions, background noise, etc.) and not always easy to define. Often, a noisy background results in a higher number of - possibly spurious - galaxy detections by SExtractor, while a worse seeing invariably results in a lower number of galaxy detections.

The large number of *class 2* detections is an indication of the large range in quality of the CCD data available for patch A. In fact, if we check the ratio of *class 2* to *class 1* objects, we get $29/41$ or, in other words, *class 2* candidates represent a percentage of $\sim 41\%$ of the total sample. Olsen et al. report, for the same ratio, $15/20$, which translates into $\sim 43\%$ of their whole sample.

Fig. 5 shows the sky distribution of our *class 1* and *class 2* candidates, circles and squares respectively.

Adding *class 1* to *class 2* candidates provides a total of 70 cluster candidates for patch A, corresponding to a surface density of 23 per square degree, with 1.3 expected spurious detections per square degree. Out of this total, 40% can be identified as richness class 0 objects and the same percentage encloses $R \sim 1$ systems, while the remaining 20% seem to be richness $R \sim 2$ clusters - see the upper panel of Fig. 8. The corresponding redshift distribution for the total Patch A sample is plotted in the upper part of Fig. 7: the distribution of *class 1* candidates does not seem to differ significantly from that of *class 2* candidates, both covering the redshift range 0.3 to 1.0 (the excess tail present for *class 2* candidates in the last redshift bin may be an artifact, due to those candidates whose m^* approaches (or would exceed) $I = 22$, the limiting magnitude of our galaxy catalogue).

Table 2. *Class 1* cluster candidates of patch A, ordered in right ascension. Coordinates $(\alpha,\delta)_{2000}$ and approximate angular size $2.5\sigma_{ang}$ (expressed in arcmin) are the mean values of the quantities issued from the even and the odd catalogues. We report values of m^*, z and $N_{0.5}$ for both the even and the odd catalogue if the discrepancy amongst at least one of the first two quantities was large or if $m_3 + 2 > 22$ (22 being our adopted magnitude limit) in the even catalogue, signalled by (e), or in the odd one, (o), or in both, (eo), making the estimate of $N_{0.5}$ quite uncertain. Some further remarks on individual entries: we note that a bright galaxy at the center in the line of sight of candidate $22^h38^m49.3^s, -39^o34'16.8''$ may have caused some (4 at the most) spurious detections, but it is hard to say as the background noise is enhanced in that area. Candidate 22 43 17.4, −39 51 54.3 is close to a large foreground spiral (ESO 345-G046) which arms were broken into pieces by the SExtractor procedure, thus producing spurious detections (see text). Finally, candidate $22^h44^m40.4^s, -39^o45'29.4''$ is near a bright star, but galaxy detections are not affected by it (maybe 4 of the objects detected in the cluster periphery are doubtful).

α_{2000}	δ_{2000}	$2.5\sigma_{ang}$	S/N_{even}	S/N_{odd}	m^*	z_{est}	$N_{0.5}$	Comments
22 35 44.4	-39 35 52.2	1.33	3.85	4.08	19.35	0.55	20	
22 35 59.4	-39 35 53.8	1.07	5.42	$\geq$ 4.34 *	18.00	0.30	15	EIS 2236-3935
22 36 01.6	-39 46 24.3	2.50	5.19	5.15	21.75	1.05	17	
22 36 17.9	-40 17 39.3	2.50	6.24	6.32	20.15	0.70	26	EIS 2236-4017
22 38 03.8	-39 34 02.1	3.54	4.16	4.06	18.45	0.40	11	EIS 2238-3934
22 38 33.4	-40 01 20.8	1.77	5.10	4.29	20.25	0.75	26	EIS 2238-4001
22 38 45.9	-39 53 18.7	1.25	4.36	4.57	19.80/19.90	0.6/0.7	21/24(eo)	EIS 2238-3953
22 38 49.3	-39 34 16.8	2.50	3.72	4.04	22.00/22.00	1.1/1.1	11/16(eo)	
22 38 55.1	-40 23 46.1	1.07	4.50	3.20	19.85	0.65	16	
22 39 16.7	-40 20 13.1	1.25	4.03	4.24	18.45	0.40	18	
22 39 34.2	-39 37 22.2	1.07	3.57	4.22	20.60/20.70	0.8/0.8	19/21(eo)	
22 40 16.5	-40 25 33.9	0.88	4.74	4.95	19.70/19.30	0.6/0.5	28/23(e)	
22 40 58.2	-40 06 12.5	3.54	5.14	4.70	20.80/21.10	0.9/0.9	35/27(e)	
22 41 16.6	-39 41 00.5	3.02	3.82	5.56	19.80/22.00	0.6/1.1	27/22	
22 41 19.7	-40 00 44.1	2.13	5.00	5.81	21.50/21.60	1.0/1.0	22/25(eo)	EIS 2241-4001
22 41 33.7	-40 20 58.1	1.25	3.67	4.30	18.45	0.40	14	
22 41 41.6	-39 49 56.7	3.54	5.91	6.86	18.50	0.40	19	EIS 2241-3949
22 43 17.4	-39 51 54.3	2.50	6.05	7.50	19.30	0.55	29	ACO1055/EIS 2243-3952
22 43 24.3	-40 25 32.8	2.13	5.27	5.94	19.00	0.50	27	EIS 2243-4025
22 43 36.1	-40 00 42.9	1.07	4.57	$\geq$ 3.93 *	18.00	0.30	14	
22 43 42.4	-39 41 48.8	3.54	3.91	4.50	18.80	0.45	16	
22 44 02.5	-40 05 19.5	0.88	4.87	4.76	20.45	0.75	20	
22 44 13.6	-39 37 05.0	1.51	3.35	4.04	20.10/19.10	0.7/0.5	19/18(e)	
22 44 19.4	-39 51 43.0	1.51	3.63	4.11	19.80/19.60	0.6/0.6	14/16(e)	
22 44 21.4	-40 08 09.2	0.88	4.08	4.20	18.70	0.40	11	
22 44 40.4	-39 45 29.4	3.02	5.67	4.75	18.80/18.90	0.4/0.5	18/21(e)	
22 44 58.5	-40 26 35.9	1.07	3.88	5.47	19.70/18.50	0.6/0.4	16/17(e)	
22 45 13.2	-39 54 09.9	0.88	4.88	5.07	19.50/19.40	0.6/0.6	12/10(e)	
22 45 34.9	-40 13 39.1	1.07	3.40	4.53	19.90/21.80	0.7/1.1	14/18	
22 45 48.1	-39 33 58.1	1.25	5.04	4.10	18.20/18.50	0.4/0.4	16/13(o)	
22 46 01.8	-39 53 50.0	3.54	4.64	4.00	22.00/22.00	1.1/1.1	7/6(o)	
22 46 12.4	-39 53 14.2	1.07	3.69	4.41	19.30/20.60	0.5/0.8	16/18	
22 46 26.9	-40 04 15.8	0.88	4.70	4.62	21.20/20.30	0.9/0.7	11/12(eo)	
22 46 48.8	-40 12 41.9	2.39	4.05	4.31	18.90	0.45	13	EIS 2246-4012
22 47 53.2	-39 35 46.8	1.51	4.26	4.22	18.60/19.40	0.4/0.6	14/14	
22 47 54.2	-39 46 33.7	1.88	5.16	4.12	22.00/19.20	1.1/0.5	12/16	LP96
22 48 27.9	-39 50 48.2	3.02	4.40	4.45	19.35	0.55	19	EIS 2248-3951
22 49 04.0	-39 42 36.5	1.33	4.05	3.04	19.20	0.55	16	
22 49 15.7	-39 37 32.6	1.07	4.39	3.77	21.20/20.60	0.9/0.8	18/16(eo)	
22 49 32.1	-39 58 04.6	0.88	4.10	4.11	20.40/20.40	0.8/0.8	13/16(eo)	EIS 2249-3958
22 49 32.7	-40 16 31.0	1.69	3.15	5.19	19.80/19.90	0.6/0.7	24/29(eo)	EIS 2249-4016

A detailed comparison of our catalogue of cluster candidates with that of Olsen et al. (1999b) will be presented in Sect. 4. Here, let us notice that in patch A there are four cluster candidates detected by previous independent works and listed in NED. Abell cluster $ACO1055$, that was selected as a *class 1* candidate by us with a high S/N. Cl2245-4002 (LP96) of Lidman & Peterson (1996) is well identified with our entry $22^h47^m54.2^s, -39^o46'33.7''$. Two EDCC cluster candidates ($EDCC163$ and $EDCC169$; Lumsden et al. 1992) do not turn up in our sample. We decided to point our algorithm directly at the NED coordinates of these two clusters while using the galaxy catalogue at $I_{lim} = 23$, just to check if their absence from our

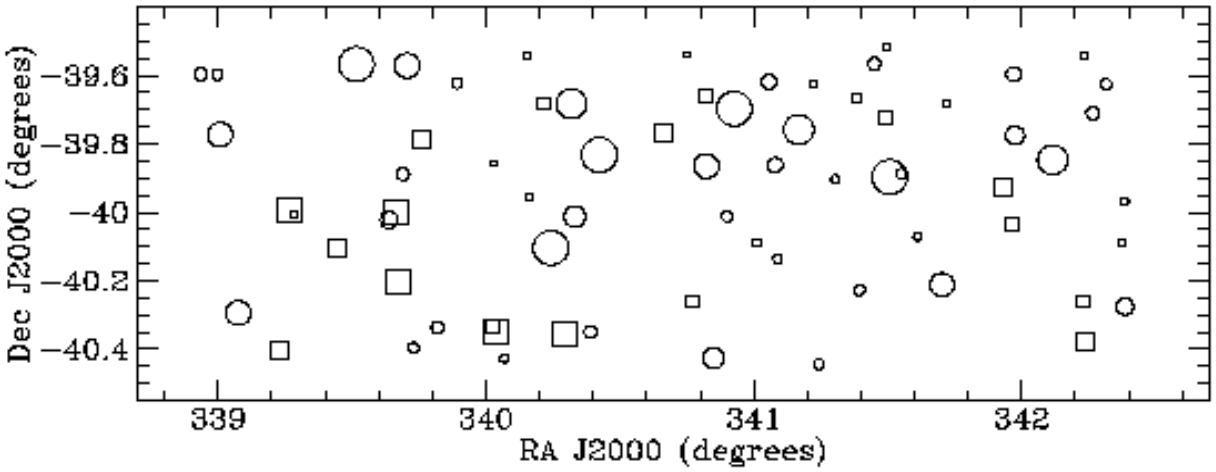

Fig. 5. Map of patch A candidates. Circles indicate *class 1* systems while squares designate *class 2* candidates. Coordinates and sizes (proportional to σ_{ang}) are mean values from even and odd catalogues. Do notice that some *class 2* candidates (namely at, roughly, (339.3^o, -40^o) and (340^o, -40.35^o)) may misleadingly appear to have escaped our double detection elimination procedure but the reason is that apparently superimposed detections are actually unmatched (*class 2*) ones flagged in different catalogues (even or odd).

Table 3. *Class 2* patch A cluster candidates. Columns and notes follow the scheme of the ones in Table 2.

α_{2000}	δ_{2000}	$2.5\sigma_{ang}$	S/N_{even}	S/N_{odd}	m^*	z_{est}	$N_{0.5}$	Comments
22 36 55.8	-40 24 11.4	1.00	-	4.08	19.90	0.7	15	
22 37 04.5	-39 59 42.4	1.41	-	4.02	18.70	0.4	16	
22 37 08.5	-40 00 22.2	0.35	-	4.50	18.00	0.3	21	EIS 2237-4000
22 37 47.2	-40 06 14.7	1.00	4.39	-	21.90	1.1	15	
22 38 38.7	-40 00 03.6	1.41	-	5.32	21.30	1.0	20(o)	
22 38 41.8	-40 12 10.8	1.41	4.10	-	21.20	0.9	12(e)	
22 39 01.6	-39 47 14.7	1.00	4.08	-	19.30	0.5	18	
22 40 06.4	-40 20 02.1	0.71	-	4.39	18.40	0.4	21	
22 40 07.4	-39 51 27.2	0.35	4.28	-	21.50	1.0	11(e)	
22 40 08.5	-40 21 01.1	1.41	5.53	-	18.70	0.4	16	EIS 2240-4021
22 40 36.2	-39 32 31.6	0.35	-	4.15	22.00	1.1	10(o)	
22 40 38.5	-39 57 27.1	0.35	-	4.24	21.00	0.9	8(o)	
22 40 51.6	-39 40 58.1	0.71	-	4.01	21.70	1.1	19(o)	
22 41 11.2	-40 21 22.3	1.41	4.18	-	18.90	0.5	11	
22 42 39.2	-39 45 56.4	1.00	-	5.27	22.00	1.1	19(o)	
22 42 59.8	-39 32 21.7	0.35	4.15	-	18.60	0.4	18	
22 43 04.6	-40 15 37.0	0.71	-	4.47	20.40	0.8	29(o)	
22 43 17.1	-39 39 33.9	0.71	4.20	-	18.80	0.4	22	
22 44 53.3	-39 37 39.2	0.35	-	$\geq$ 4.66 *	18.00	0.3	27	
22 45 33.1	-39 39 52.7	0.50	-	$\geq$ 4.24 *	18.00	0.3	35	
22 45 58.5	-39 31 04.8	0.35	4.07	-	21.20	0.9	7(e)	
22 45 58.6	-39 43 21.3	0.71	-	$\geq$ 4.69 *	18.10	0.3	29	
22 46 53.0	-39 41 03.4	0.35	-	4.07	21.70	1.1	7(o)	
22 47 43.2	-39 55 29.7	1.00	4.33	-	21.10	0.9	8	
22 47 52.1	-40 02 05.6	0.71	-	4.03	19.30	0.5	15	
22 48 55.3	-40 15 37.0	0.71	-	4.02	18.00	0.3	13	EIS 2248-4015
22 48 56.7	-39 32 32.3	0.35	4.52	-	19.70	0.6	20	
22 48 57.6	-40 22 44.7	1.00	4.59	-	20.50	0.8	26	
22 49 29.2	-40 05 27.7	0.35	4.17	-	22.00	1.1	12(e)	

list could be due to the magnitude cut–off chosen. This approach managed to retrieve $EDCC169$ with $S/N_{even} = 3.29$ and $S/N_{odd} = 3.84$, while $EDCC163$ is still missing. According to the Lumsden et al. (1992) table, both candidates are considered to be poor R < 0 systems, which may account for our results.

Out of these 4 objects, only Abell $ACO1055$ has spectroscopic confirmation (at $z = 0.0322$) and, consequently, a re-

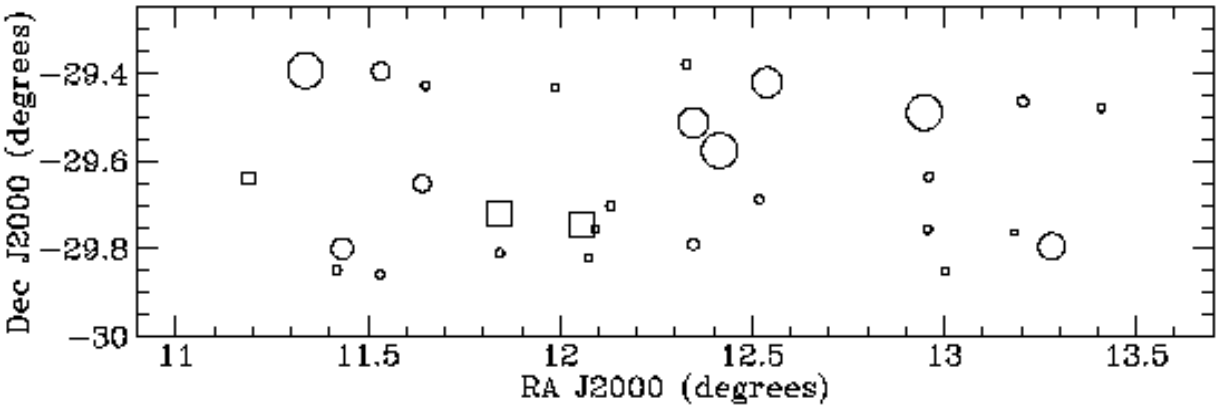

Fig. 6. Same as Fig. 5 but for patch B candidates.

liable richness estimate ($R = 0$) in the literature (cf. NED database). The redshift we estimate for this system is higher ($z_{even} = 0.6$, $z_{odd} = 0.5$) and the richness we compute ($R \simeq 2$) is, consequently, considerably incorrect. Notice though that visual inspection indicates that a lot of spurious "galaxies" were detected by SExtractor in the spiral arms of the foreground bright galaxy ESO 345-G046 (the effect is more serious for the even catalogue), and this has possibly affected our results, namely the determination of m^*.

3.3.2. Patch B

Class 1 candidates in patch B total 21, which translates into $\Sigma \sim 15$ clusters per square degree (this patch covers, approximately, 1.4 square degrees). This is a slightly higher density than that found for patch A, possibly because of better data quality (patch B had better observing conditions). Note that Olsen and collaborators also find some difference: they report 14 clusters per square degree in patch A while the value rises to 17.2 for patch B. This difference between both patches is, however, negligible within uncertainties.

Table 4 lists, with the same format already used for patch A candidates, our *class 1* patch B cluster candidates.

The simulations of Sect. 2.5 allow us to predict $1.3 \times 1.4 \sim 2$ spurious detections associated to the 21 candidates.

Very much like for patch A, in 71% of the cases (15 out of 21), the redshift estimates from the even and odd catalogues differ in absolute value of less than 0.1.

As for *class 2* candidates in this patch, Table 5 lists all 8 detections that survived accurate visual inspection.

Fig. 6 shows the sky distribution of our *class 1* and *class 2* candidates, respectively.

Also for patch B holds the discussion already made for *class 2* candidates in patch A. It is to be noticed that now the ratio of *class 2* to *class 1* candidates is much lower than the one obtained for patch A: $8/21$ or a percentage of 28% of the total sample (*versus* the previous 41%), suggesting that the quality of the CCD data available for patch B is indeed much more homogeneous. We note here that the same type of ratio produced

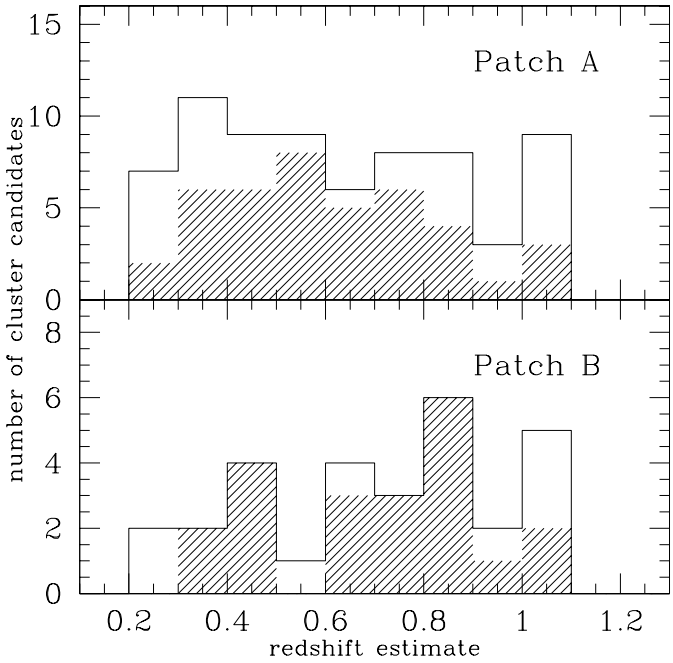

Fig. 7. Redshift distribution for the cluster candidates flagged in patch A - upper panel - and patch B - lower panel. Hatched histograms specify matched ($class1$) detections among the global distribution (empty histograms). In this figure the z plotted for each cluster candidate is the mean value obtained from even and odd catalogues.

with Olsen et al.'s candidates for this patch is $9/10$ or, in terms of percentage of their whole sample, $\sim 47\%$, which remains quite similar to the figure they produce for patch A.

Adding *class 1* to *class 2* candidates gives a total of 29 cluster candidates in patch B, corresponding to a surface density of ~ 21 per square degree, with, again, the already mentioned 1.3 expected spurious detections per square degree. Out of these 29 systems, 62% have estimated richness class $R \sim 0$, and 38% have $R \sim 1$, as illustrated in the lower panel of Fig. 8. Notice that, the area probed here being smaller than the one of Patch A, at the same limiting magnitude this translates into a smaller sampled volume. So it is expected that the median typical richness of the detected systems should move to lower

Table 4. *Class 1* cluster candidates of patch B, ordered in right ascension. Quantities listed and notes used are equivalent to those reported in Table 2. Candidate $00^h51^m50.5^s, -29^o38'05.3''$ is near a bright star (and 4 of the objects detected in the cluster periphery are doubtful).

α_{2000}	δ_{2000}	2.5 σ_{ang}	S/N_{even}	S/N_{odd}	m^*	z_{est}	$N_{0.5}$	Comments
00 45 21.0	-29 23 35.5	3.54	$\geq$ 6.34 *	$\geq$ 7.32 *	18.40	0.40	24	EIS 0045-2923
00 45 40.5	-29 50 54.2	0.88	4.48	3.91	20.60/19.70	0.8/0.6	18/16(eo)	
00 45 44.0	-29 47 57.5	2.13	4.81	4.67	22.00/19.10	1.1/0.5	17/23	EIS 0045-2948
00 46 07.5	-29 51 28.7	0.88	3.99	4.39	20.05	0.70	17	EIS 0046-2951
00 46 08.1	-29 23 40.8	1.77	3.90	4.50	18.95	0.45	19	
00 46 33.9	-29 39 03.2	1.69	4.90	3.95	21.10/20.00	0.9/0.7	22/18 (eo)	
00 46 35.9	-29 25 38.8	0.88	4.03	3.34	18.90/18.70	0.5/0.4	7/7(e)	
00 47 22.3	-29 48 33.7	0.88	4.49	3.72	21.20/20.80	0.9/0.9	19/14(eo)	
00 48 31.6	-29 42 06.6	0.88	4.34	4.34	20.80	0.85	15	EIS 0048-2942
00 49 19.0	-29 22 45.2	0.88	3.21	4.03	18.95	0.45	8	
00 49 23.2	-29 30 43.0	3.02	5.00	5.56	18.55	0.40	19	ACO84/EIS 0049-2931
00 49 23.3	-29 47 21.4	1.07	3.14	4.25	20.30/20.30	0.7/0.7	11/17(eo)	
00 49 39.5	-29 34 33.1	3.54	5.76	5.63	18.85	0.45	9	
00 50 04.5	-29 41 13.5	0.88	3.88	4.71	21.40/22.00	1.0/1.1	12/13(eo)	EIS 0050-2941
00 50 09.4	-29 25 12.4	3.02	3.43	4.29	20.30/22.00	0.7/1.1	9/17(eo)	
00 51 47.6	-29 29 20.2	3.54	5.19	4.97	21.05	0.90	8	
00 51 49.6	-29 45 20.1	0.88	4.21	4.29	20.10/20.50	0.7/0.8	11/15(o)	
00 51 50.5	-29 38 05.3	0.88	4.76	3.36	21.80/19.90	1.1/0.7	13/4(eo)	
00 52 49.3	-29 27 49.5	1.07	4.83	4.18	21.80/21.90	1.1/1.1	17/15(eo)	EIS 0052-2927
00 53 07.1	-29 47 40.7	2.65	4.04	3.43	21.50/20.60	1.0/0.8	11/11(o)	
00 53 38.1	-29 28 41.8	0.88	3.00	4.09	21.10/21.50	0.9/1.0	12/9(eo)	

Table 5. *Class 2* patch B cluster candidates. Columns and notes are the same that were used in Table 4.

α_{2000}	δ_{2000}	2.5 σ_{ang}	S/N_{even}	S/N_{odd}	m^*	z_{est}	$N_{0.5}$	Comments
00 44 45.0	-29 38 17.1	0.71	4.18	-	21.30	1.0	20(e)	
00 47 21.9	-29 43 16.9	1.41	-	4.90	19.70	0.6	11	
00 47 56.7	-29 26 00.1	0.35	-	4.68	22.00	1.1	9(o)	
00 48 13.5	-29 44 44.3	1.41	$\geq$ 4.21 *	-	18.00	0.3	12	
00 48 18.2	-29 49 09.5	0.35	-	4.27	20.10	0.7	11	
00 48 22.1	-29 45 21.4	0.35	5.25	-	18.00	0.3	18	
00 52 00.5	-29 50 58.3	0.35	-	4.00	21.80	1.1	11(o)	
00 52 43.6	-29 45 45.3	0.35	4.18	-	21.70	1.1	14(e)	

values. The corresponding total redshift distribution is plotted in the bottom of Fig. 7. The median of the redshift distribution for *class 1* candidates, patch A and B considered together, is $z = 0.65$, similar to that of Olsen et al. despite having chosen a brighter cut–off in magnitude for the galaxy catalogue (22 *versus* their 23), while it is slightly deeper than that of the P96 sample PDCS ($z = 0.4$).

There is only one cluster candidate in patch B detected by previous independent works and listed in NED. It is cluster $ACO84$, that was selected as a *class 1* candidate by us. We estimate 0.40 for the redshift of this candidate (and a corresponding richness class $R \sim 1$), while spectroscopic measurements in the literature hold a value of $z = 0.11$ (cf. the NED database) and $R = 0$. Also for patch B, a more detailed comparison between our catalogue of cluster candidates and that of Olsen et al. (1999a) will be presented in Sect. 4.

4. Comparison with Olsen et al.'s results

We can now do a thorough comparison with the results that Olsen et al. (1999a, 1999b) obtained by applying the P96 algorithm to patches A and B of EIS. In this way we will also be able to assess directly the relative efficiency of the two algorithms (P96 and ours) on the same set of data.

We will have to do a double check: first which of our candidates are new with respect to the Olsen et al. lists, and then which of the Olsen et al. candidates are missing from our lists.

For the comparison to be fair, we have to remember three important points: Olsen and co-workers did their search on the total galaxy catalogue, i.e. up to magnitude $I = 23$, while we preferred to limit it to $I = 22$. They applied a S/N cut–off of 3, while we adopted a S/N cut–off of 4 in our final cluster list and, finally, they also imposed a cut–off in richness to their candidates, while we apply no such sort of selection.

Bearing this in mind, we proceed with the comparisons.

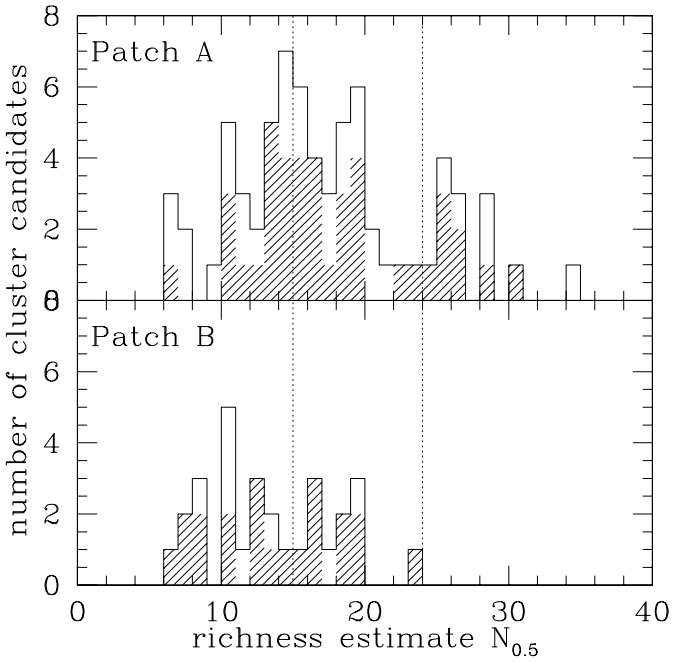

Fig. 8. Distribution of the richness estimate $N_{0.5}$ for the cluster candidates flagged in patch A - upper panel - and patch B - lower panel. Hatched histograms specify matched detections among the global distribution (empty histograms). The dotted lines mark the approximate limits between Abell richness classes 0 and 1 (at $N_{0.5} \sim 15$) and Abell richness classes 1 and 2 ($N_{0.5} \sim 24$). The $N_{0.5}$ plotted for each cluster candidate is the mean value obtained from even and odd catalogues.

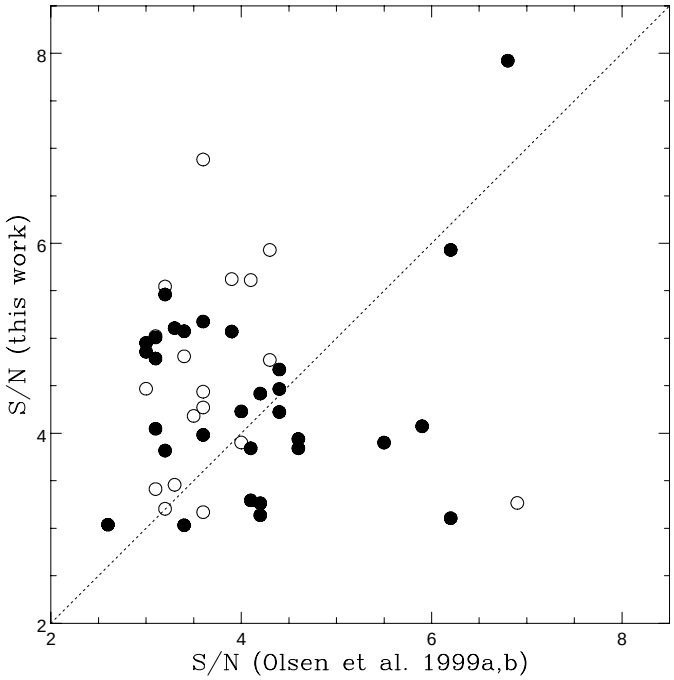

Fig. 9. S/N obtained with our algorithm for the Olsen et al. (1999a,b) candidates *versus* their own S/N. Filled symbols stand for patch A objects while patch B candidates are noted by empty symbols. The $S/N_{Olsen} = S/N_{us}$ line is also marked.

Regarding patch A, in our *class 1* list we have 13 candidates in common with Olsen et al. (1999b), while in the *class 2* list we have only 3 candidates in common. Out of our remaining candidates, 6 from *class 1* and 9 from *class 2* are in an area of patch A that they decided to cut–out from their search (the upper right corner of their Fig. 2) because of *"obvious incompleteness" (sic)*. We did search also in this area, since our algorithm, using local background values, is better suited for dealing with inhomogeneous data. We therefore are left with 22 *class 1* candidates and 17 *class 2* candidates present in our list and missing in theirs. Some of these missing candidates might have been discarded by Olsen et al. (1999b) because of the richness cut–off they imposed, but it should be noticed that amongst them there are also relatively rich systems: 5 with estimated richness $R \sim 2$ and 25 with richness $R \sim 1$ (conservatively counting only our $N_{0.5}$ secure values), whose absence is thus not easy to justify.

In what concerns patch B, we only have 7 candidates in common with Olsen et al. (1999a), all in our *class 1* list. We are therefore left with 14 *class 1* candidates and all 8 *class 2* candidates present in our catalogues and missing in theirs.

On the other hand, there are candidates present in the Olsen et al. lists that we failed to select, and we wanted to check if our missing them could be related to the different magnitude cut–off of the galaxy catalogue used for our search or to the different S/N cut–off adopted.

To investigate this we decided to check which would have been the S/N obtained for these missing candidates by our algorithm on the galaxy catalogue limited to their deeper magnitude cut–off ($I = 23.0$). To do this we simply targeted directly the search to the positions of each one of their candidates.

By doing so, we were able to retrieve all their patch A candidates with a $S/N \geq 3$ in at least the even or the odd catalogue (the same selection criterion they adopted), with the only exception of four of them. One of those was commented by Olsen et al. as being a *"doubtful case based on the visual inspection of the coadded image"* and to another one our algorithm could only attribute a lower limit S/N (from the spatial part).

In patch B, with the same procedure, we assigned all their candidates a $S/N \geq 3\sigma$ except for three (one of them being also a case of lower limit S/N obtained from the spatial filtering).

The plot of our S/N against theirs, for all the candidates we retrieved (common candidates), is shown in Fig. 9, both for patch A (filled symbols) and patch B (empty symbols) objects.

One can notice that, for the majority of the cases, our S/N is greater than that obtained by Olsen et al. as would be expected: by decoupling the spatial and the luminosity parts of the algorithm, a candidate can be retrieved even when it does not flag a maximum likelihood at the very same redshift value simultaneously for both distributions, a situation that would lower its global likelihood when using the P96 algorithm.

Another interesting plot is the one showing, for the common candidates, our m^* estimate *versus* the redshift estimate by Olsen et al. (1999a, 1999b). Fig. 10 plots the mean value (from the even and the odd catalogues) of m^* produced by our

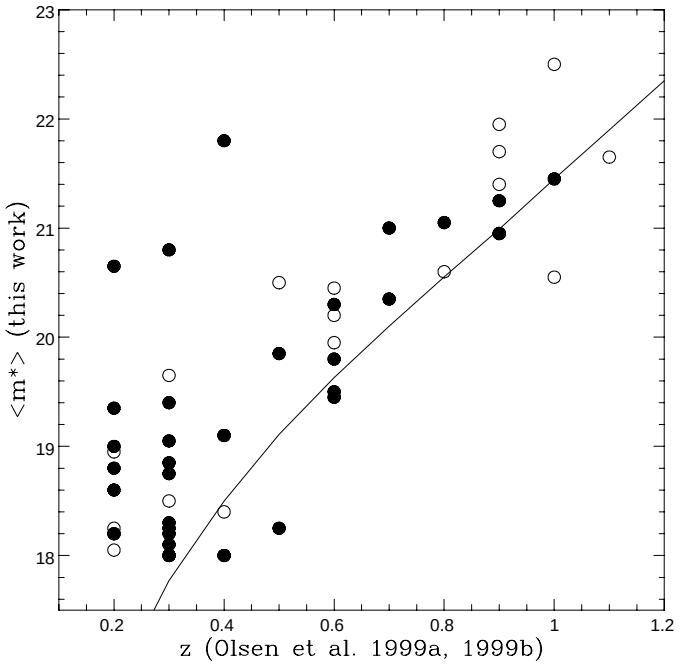

Fig. 10. Checking the possibility of correlation between our m^* (average value from even and odd catalogues) and Olsen et al.'s redshift estimate for their candidates in patch A (filled symbols) and in patch B (empty symbols). The line is the relation deduced from Colless (1989).

algorithm against the redshift estimated by Olsen et al. for their candidates in patch A (filled circles) and in patch B (empty circles). The line indicates the redshifted value of the Colless (1989) local mean m^*, affected by k–correction typical of ellipticals (as determined by Fioc & Rocca-Volmerange 1997). The general distribution of the data points does seem to follow the curve's trend. The larger redshift systematically predicted by the Colless relationship we used is just a byproduct of the brighter M^* estimated by Colless ($I^* \simeq -22.2$ for $H_0 = 100$ km s^{-1}Mpc^{-1}) *versus* the one used in P96 and by Olsen et al. (-21.28, also for $H_0 = 100$ km s^{-1}Mpc^{-1}). This fact may also be contributing to the discrepancies between our estimates and the literature measures in the case of the Abell clusters mentioned in Sect. 3.3.

5. Summary and conclusions

In this paper we presented a new algorithm for cluster detection that improves on the P96 one, mainly by avoiding the need to assume a typical physical size or a typical M^* for galaxy clusters. These two parameters intervene in our algorithm only as typical angular scales and a typical apparent magnitude m^*, bearing no ties to fixed physical scales nor to absolute magnitudes through redshift dependence (and chosen cosmological model). One further advantage of our algorithm with respect to P96's consists in the local estimate of the background for each cluster candidate, particularly useful in the spatial part where local inhomogeneities (due to varying conditions during data acquisition) may hamper cluster detection in shallower regions of the catalogue.

We applied this new algorithm to the EIS-wide database and did a thorough comparison with the results obtained using P96 on the same kind of data. As the EIS observing conditions varied considerably throughout the granted nights, there was a considerable spread in the data-quality of different EIS frames (Nonino et al. 1999). Both the particular features of the algorithm presented in this paper, that somehow compensate for the lack of homogeneity of the data, and the conservative limiting magnitude adopted for cluster search try to minimize the problems inherent to the EIS data, allowing to achieve a higher completeness level than that obtained using P96 on the same data.

In fact, we notice that the distribution of our patch A candidates seems more homogeneous than the one presented by Olsen et al. (1999b): compare our Fig. 5 with their Fig. 4, where they have a region around $\alpha^o \sim 341.5$, $\delta^o \sim -40$ devoid of detections, not to mention the fact that they intentionally left out a part of the patch when running their algorithm to "overcome" data problems related to the lack of homogeneity.

Regarding the cluster candidate surface density, a precise comparison with the values presented in the literature is not trivial, due to different magnitude limits adopted for the search and to the fact that we did not apply any *a priori* selection on cluster richness (as P96 for example). Just as a qualitative comparison, let us remember that the PDCS group (P96) reports the detection of 79 cluster candidates over an area of 5.1 square degrees till $I = 22.5$, or a number density slightly above 15. This value is consistent with the observed X–ray $logN - logS$ around fluxes $> 6^{-15}$ erg cm^{-2} s^{-1} (see Fig. 3 of Rosati 1998). In this paper, adding *class 1* to *class 2* candidates both for patch A and B we obtain a surface density of ~ 22 clusters per square degree, out of which $\sim$ 54% have $R = 1$ or above, which agrees well, within the uncertainties, with the number quoted by the PDCS group, possibly suggesting a slightly larger surface density for our candidates, especially when taking into account the deeper magnitude limit adopted for the search by the PDCS group.

We are doing multicolor (B, V, R and I) observations of the sample of cluster candidates presented in this paper using the 3.6-m and NTT ESO telescopes. Redshift confirmation of three of our high redshift ($z \sim 0.65$) candidates has already been obtained using FORS at the VLT, confirming the efficiency of the strategy adopted.

Acknowledgements. It is a pleasure to thank L. Guzzo for discussions and comments. C. Lobo acknowledges main financial support by the CNAA fellowship reference D.D. n.37 08/10/1997, and also the FCT PRAXIS XXI fellowship BPD/20174/99, and the ESO/PRO/15130/1999. This research has made use of the NASA/IPAC Extragalactic Database (NED) which is operated by the Jet Propulsion Laboratory, California Institute of Technology, under contract with the National Aeronautics and Space Administration.

References

Abell G.O., 1958, ApJS 3, 211
Alonso M.V., Valotto C., Lambas D.G., Muriel H., 1999, MNRAS 308, 618

Bahcall N., 1981, ApJ 247, 787
Bahcall N., 1988, ARA&A 26, 631
Bahcall N., Fan X., Cen R., 1997, ApJ 485, L53
Bartelmann M., Huss A., Colberg J.M., Jenkins A., Pearce F.R., 1998, A&A 330, 1
Böhringer H., Guzzo L., Collins C.A., et al., 1998, In: Colombi, Mellier, Raban (eds.) Proceedings of Wide Field Surveys in Cosmology. astro-ph/9809381
Campos A., Yahil A., Windhorst R.A., et al., 1999, ApJ 511, L1
Carlberg R.G., Morris S.L., Yee H.K.C., Ellingson E., 1997, ApJ 479, L19
Castander F.J., Bower R.G., Ellis R.S, et al., 1995, Nature 377, 39
Colless M., 1989, MNRAS 237, 799
Collins C.A., Burke D.J., Romer A.K., Sharples R.M., Nichol R.C., 1997, ApJ 479, L117
Couch W.J., Ellis R.S., Malin D.F., MacLaren I., 1991, MNRAS 249, 606
Dalcanton J.J., 1996, ApJ 466, 92
Dalton G.B., Efstathiou G., Maddox S.J., Sutherland W.J., 1994, MNRAS 269, 151
Deltorn J.–M., Le Fèvre O., Crampton D., Dickinson M., 1997, ApJ 483, L21
Dickinson M., 1996, Proceedings of HST and the high-z Universe, astro-ph/9612178
Dressler A., Oemler A., Couch W.J., et al., 1997, ApJ 490, 577
Ebeling H., Edge A.C., Böhringer H., et al., 1998, MNRAS 301, 881
Escalera E., MacGillivray H.T., 1995, A&A 298, 1
Escalera E., MacGillivray H.T., 1996, A&AS 117, 519
Fadda D., Slezak E., Bijaoui A., 1998, A&AS 127, 335
Fioc M., Rocca-Volmerange B., 1997, A&A 326, 950
Fukugita M. Shimasaku K., Ichikawa T., 1995, PASP 107, 945
Gal R.R., de Carvalho R.R., Odewahn S.C., Djorgovski S.G., Margoniner V.E., 2000, AJ 119, 12
Gioia I.M., 1997, Proceedings of The Young Universe. astro-ph/9712003
Gladders M.D., Yee H.K.C., 2000, AJ submitted, astro-ph/0004092
Henry J.P., Gioia I.M., Maccacaro T., et al., 1992, ApJ 386, 408
Henry J.P., Gioia I.M., Mullis C.R., 1997, AJ 114, 1293
Jones M.E., Saunders R., Baker J.C., et al., 1997a, ApJ 479, L1
Jones L.R., Scharf C.A., Ebeling H., et al., 1997b, ApJ 495, 100
Kepner J., Fan X., Bahcall N., et al., 1999, ApJ 517, 78
Kawasaki W., Shimasaku K., Doi M., Okamura S., 1998, A&AS 130, 567
Le Fèvre O., Deltorn J.–M., Crampton D., Dickinson M., 1996, ApJ 471, L11
Lidman C.E., Peterson B.A., 1996, AJ 112, 2454
Lumsden S.L., Nichol R.C., Collins C.A., Guzzo L., 1992, MNRAS 258, 1
Mendes de Oliveira C., Hopp U., Bender R., Drory N., Saglia R.P., 1998, In: Barbuy B. (ed.) Proceedings of Science with Gemini. astro-ph/9810021
Morris S.L., Hutchings J.B., Carlberg R.G., et al., 1998, ApJ 507, 84
Nonino M., Bertin E., da Costa L., et al., 1999, A&AS 137, 51
Olsen L.F., Scodeggio M., da Costa L., et al., 1999a, A&A 345, 363
Olsen L.F., Scodeggio M., da Costa L., et al., 1999b, A&A 345, 681
Ostrander E.J., Nichol R.C., Ratnatunga K.U., Griffiths R.E., 1998, AJ 116, 2644
Pascarelle S.M., Windhorst R.A., Driver S.P., Ostrander E.J., Keel W.C., 1996, ApJ 456, L21
Pisani A., 1996, MNRAS 278, 697
Postman M., Lubin L.M., Gunn J.E., et al., 1996, AJ 111, 615
Ramella M., Nonino M., Boschin W., 1998, In: Giuricin G., Mezzetti M., Salucci P. (eds.) Proceedings of Observational Cosmology: The Development of Galaxy Systems. ASP Conference Ser., astro-ph/9810124
Renzini A., da Costa L., 1997, The Messenger No 87, p. 23
Richards E.A., Fomalont E.B., Kellermann K.I., Partridge K.I., Windhorst R.A., 1997, AJ 113, 1475
Rosati P., 1998, In: Colombi, Mellier, Raban (eds.) Proceedings of Wide Field Surveys in Cosmology. astro-ph/9810054
Rosati P., Della Ceca R., Burg R., Norman C., Giacconi R, 1995, ApJ 445, L11
Rosati P., Della Ceca R., Norman C., Giacconi R, 1998, ApJ 492, L21
Scharf C.A., Jones L.R., Ebeling H., et al., 1997, ApJ 477, 79
Schuecker P., Böhringer H., 1998, A&A 339, 315
Schechter P., 1976, ApJ 203, 297
Shectman S.A., 1985, ApJS 57, 77
Smail I., Edge A.C., Ellis R.R., Blandford R.D., 1998, MNRAS 293, 124
Stanford S.A., Elston R., Eisenhardt P.R., et al., 1997, AJ 114, 2232
Stanford S.A., Eisenhardt P.R., Dickinson M., 1998, ApJ 492, 461
Sunyaev R.A., Zel'dovich Ya.B., 1980, ARA&A 18, 537
van Dokkum P.G., Franx M., Kelson D.D., Illingworth G.D., 1998a, ApJ 504, L17
van Dokkum P.G., Franx M., Kelson D.D., et al., 1998b, ApJ 500, 714
Viana P.T.P., Liddle A.R., 1996, MNRAS 281, 323
Vikhlinin A., McNamara B.R., Forman W., et al., 1998a, ApJ 498, L21
Vikhlinin A., McNamara B.R., Forman W., et al., 1998b, ApJ 502, 558
Zaritsky D., Nelson A.E., Dalcanton J.J., Gonzalez A.H., 1997, ApJ 480, L91